NEUTRON IMAGING, RADIOGRAPHY AND TOMOGRAPHY*

Graham C. Smith
Brookhaven National Laboratory
Upton, NY 11973-5000

March, 2002

* Work supported by U.S. Department of Energy: Contract No. DE-AC02-98CH10886.

NEUTRON IMAGING, RADIOGRAPHY AND TOMOGRAPHY *

Graham C. Smith
Instrumentation Division
Brookhaven National Laboratory
Upton, NY 11973-5000

Abstract

Neutrons are an invaluable probe in a wide range of scientific, medical and commercial endeavors. Many of these applications require the recording of an image of the neutron signal, either in one-dimension or in two-dimensions. We summarize the reactions of neutrons with the most important elements that are used for their detection. A description is then given of the major techniques used in neutron imaging, with emphasis on the detection media and position readout principle. Important characteristics such as position resolution, linearity, counting rate capability and sensitivity to gamma-background are discussed. Finally, the application of a subset of these instruments in radiology and tomography is described.

* This work was supported by the U.S. Department of Energy: Contract No DE-AC02-98CH10886

Key Words:
Neutron, Radiation, Detector, Imaging, Gas, Silicon, Scintillator

Submitted for inclusion in:
Encyclopedia of Imaging Science and Technology
John Wiley & Sons, Inc.
July 2001

Blank Page

NEUTRON IMAGING, RADIOGRAPHY AND TOMOGRAPHY

Graham C. Smith
Brookhaven National Laboratory
Upton, NY 11973-5000

1. Introduction.

The discovery of the neutron occurred in 1932 and the first neutron diffraction experiments were performed in the late 1940s. With progressively increasing usage, the neutron has become a key probe in many fields of science, with sources around the world now over-subscribed by experimenters. The European Spallation Source, ESS, and the Spallation Neutron Source, SNS, in the US are new, high intensity sources under development that attest to the importance of neutrons as a probe. Because they are uncharged, neutrons are perhaps one of the most difficult of particle to detect. Indeed, there are only a few elements in nature that have a high affinity for neutron interaction. This article is organized as follows. In section 2 the fundamental reactions upon which all neutron detection relies are described. Then a series of sections describe the main techniques of neutron detection and imaging: gas-based in section 3, scintillator based in section 4, semiconductor-based in section 5, film and image plates in section 6 and microchannel plates in section 7. In these sections a few applications are noted. Section 8 focuses on neutron radiography/tomography, for which scintillator detectors and image plates are the primary imaging techniques. Some important reviews from recent literature are, for imaging techniques: Convert (1983), Crawford (1992), Fraser (1995), Lander (1996), Hastings (1998), and for radiography: Fischer (1996), Lehmann (1999). Techniques for (non-imaging) neutron detection have also recently been reviewed (Peurrung, 2000), and an excellent treatise on all neutron detectors is given in Knoll (1989).

2. Neutron Interaction Mechanisms.

Creation of free charge carriers is the primary process upon which most radiation detectors rely for their operation. Neutrons have no net charge, and can be detected either by direct collision with, and displacement of, nuclei, or by nuclear interactions. For thermal neutrons, there is insufficient energy available for collision displacements, and nuclear reactions are the dominant process in neutron detection methods. With definitions for cold, thermal and epithermal neutrons indicated, figure 1 shows the neutron absorption cross-section versus energy for the most important capture reactions, which can be loosely categorized in three groups:

i) Reactions that have cross-sections that decrease as the square root of the neutron energy:

$^{3}He + {}^{1}n \rightarrow {}^{3}H + {}^{1}H + 0.764$ MeV
$^{6}Li + {}^{1}n \rightarrow {}^{4}He + {}^{3}H + 4.8$ MeV
$^{10}B + {}^{1}n \rightarrow {}^{7}Li + {}^{4}He + 2.3$MeV $+ 0.48$ MeV (γ)

ii) Reactions that are (n,γ) resonances in which γ-ray emission is inhibited and energy is transferred to the orbital electrons. This class of reactions gives rise to complex γ-ray and conversion electron spectra (Groshev, 1962):

$^{155}Gd + {}^{1}n \rightarrow {}^{156}Gd^*$

$\rightarrow {}^{156}Gd + (\gamma +$ conversion e's; 7.9 MeV)

Main electron energies are 39 and 81 keV

$^{157}Gd + {}^{1}n \rightarrow {}^{158}Gd^*$

$\rightarrow {}^{158}Gd + (\gamma$'s + conversion e's; 8.5 MeV)

Main electron energies are 29, 71, 78 and 131 keV

iii) Fission of ^{235}U or ^{239}Pu:

$^{235}U + {}^{1}n \rightarrow$ fission fragments + 80 MeV

$^{239}Pu + {}^{1}n \rightarrow$ fission fragments + 80 MeV

A common feature of the reactions in (i) is that the products are ejected co-linearly, and in general give rise to ionizations within several μm (solid) or mm (gas) of the reaction point; in lithium the range is about 100μm. The (n,γ) reactions in (ii) have a high probability of internal conversion, and the conversion electrons ejected are much more easily stopped than γ-rays, providing much more accurate position information. Although ^{113}Cd has a high neutron capture cross-section (figure 1), it has not been included in (ii) because it has a low probability of internal conversion (about 4% of that for Gd) and accurate position information is difficult to obtain. The reactions in (iii) are based on nuclear fission. Their energies are very high, but the relatively low cross-sections and difficulties with isotope enrichment have resulted in little use of these reactions. A compendium of neutron cross-sections for many elements in the periodic table has been published by Garber and Kinsey (1976).

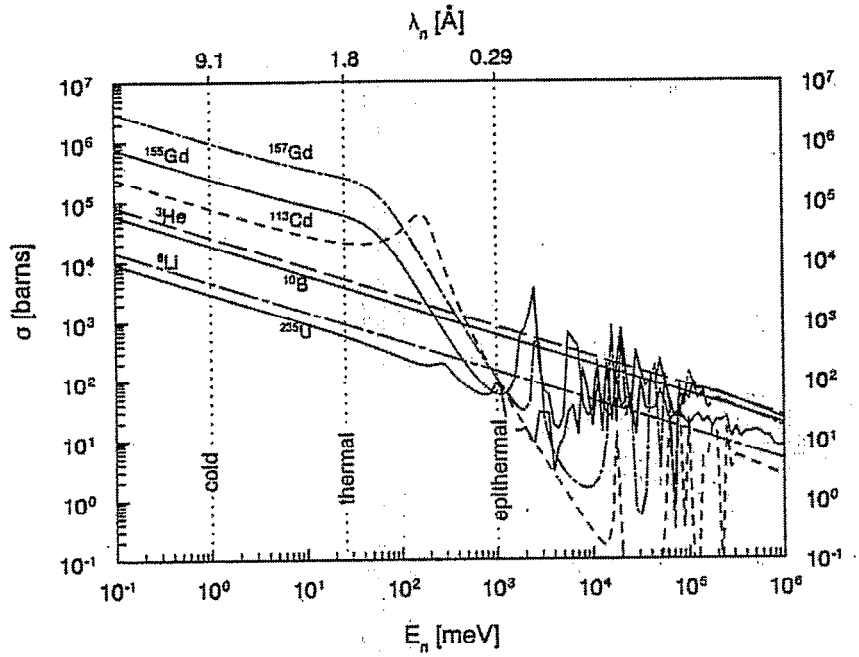

Figure 1. Cross-sections for the most important neutron capture reactions versus neutron energy

Two of the most important characteristics of a neutron imaging device are position resolution and efficiency. The (useful) isotopes in (i) and (ii) above are shown in table 1, in their most common physical forms. Information pertaining to reaction product energies and ranges, and absorption depth for neutrons with energy 0.025 eV (1.8Å) is also given. These numerical values are most valuable in determining the isotope's utilization in position-sensitive detectors.

Table 1

The most useful neutron absorbing isotopes and the key features of the neutron interactions at 25meV. Cross sections, σ_n, are tabulated to the nearest 10 barns, and to the nearest 1000 barns for Gd. This helps emphasize the huge stopping power of Gd relative to the other isotopes.

Isotope	State	σ_n (barns)	Neutron abs^n. length	Particle energies (keV)		Approximate particle range
^{3}He	Gas	5330	70 mm.atm	p: 573	t: 191	3.8 mm.atm C_3H_8
^{6}Li	Solid	940	230 μm	t: 2727	α: 2055	130 μm
^{10}B	Solid	3840	20 μm	α: 1472	^{7}Li: 840	3 μm
$^{10}BF_3$	Gas	3840	97 mm.atm	α: 1472	^{7}Li: 840	4.2 mm.atm
Nat. Gd	Solid	49000	6.7 μm	Conv^n electrons: ~30-200		12 μm
^{157}Gd	Solid	254000	1.3 μm	Conv^n electrons: ~30-200		12 μm

3. Detectors with Gas-Filling.

Before gas-filled imaging detectors were developed, the usual component in single wire proportional counters for neutron detection was boron trifluoride, BF_3. In recent years ^{3}He has become the converter gas of choice because BF_3 is not an ideal gas in which to multiply electrons, and even with enrichment in ^{10}B, the absorption cross-section is significantly smaller than that of ^{3}He.

The gas depth in a thermal neutron proportional chamber is typically 10-15 mm. This is a compromise between achieving high efficiency and minimizing position error due to parallax for neutrons incident away from the normal to the detector. Figure 2 shows the calculated detection efficiency in 15 mm for a range of gas pressures. Extremely high detection efficiencies can be obtained for cold neutrons, around 8-10 Å.

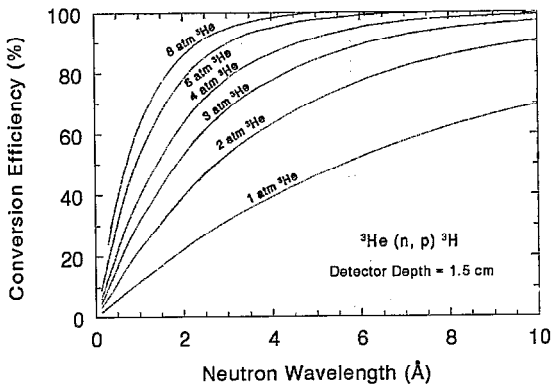

Figure 2. Calculated thermal neutron conversion efficiency for a range of ^{3}He partial pressures.

Ultimately, the major factor limiting position resolution for neutron conversion in ^{3}He is the range of the proton and triton. Figure 3 shows the relative dE/dX profile of the proton and triton as a function of distance from the interaction point. The proton not only takes about three-quarters of the reaction energy, but also deposits a disproportionate quantity of ionization at the end of its track. The center of gravity of the resulting primary ionization is weighted, unfortunately, part way along the proton track, typically 0.35 R_p from the interaction point, where R_p is the range of the proton. A key parameter in obtaining high resolution is to ensure that the proton and triton ranges are kept small. This is normally achieved by using a heavier gas such as propane, C_3H_8, or carbon tetra-fluoride, CF_4, as an admixture with the ^{3}He. These gases also act as a quench for the electron avalanche.

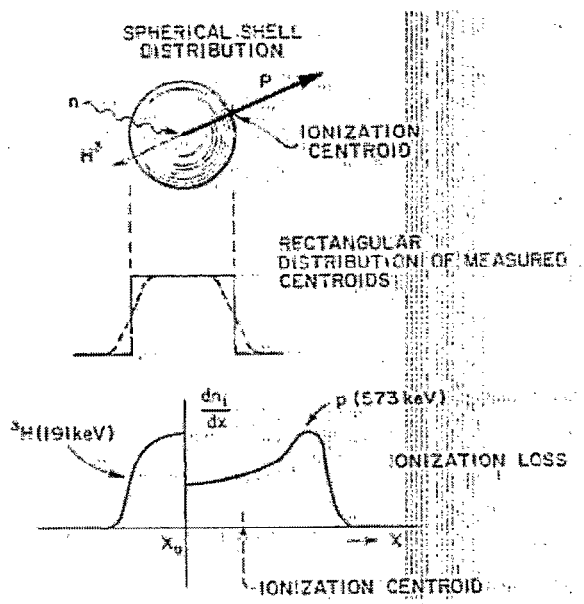

Figure 3. Representation of sphere of centroids from many conversions. Ionization centroid is displaced from conversion point by about $0.4 \times R_p$, the proton range.

Figure 4 shows the manner in which propane improves the position resolution as a function of its pressure (Radeka, 1996).

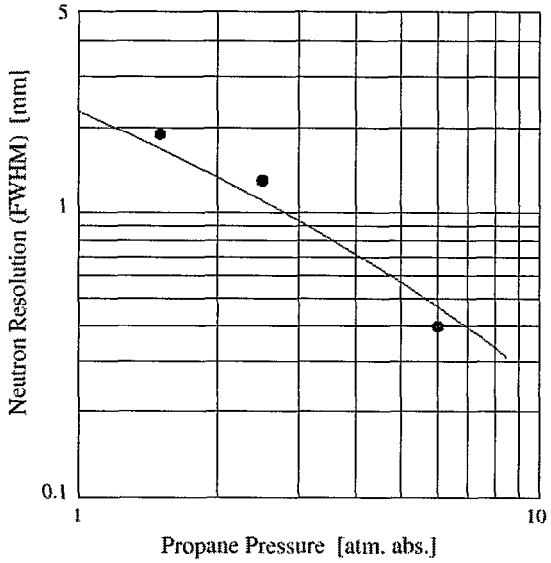

Figure 4. Position Resolution in $^3He + C_3H_8$ as a function of absolute propane pressure.

i) Multi-Wire Proportional Chambers (MWPCs).

The concept of the multi-wire chamber was born over 30 years ago (Charpak, 1968), but its application in a variety of radiation detection applications is ubiquitous even today; neutron detection is no exception. Figure 5 shows schematically a typical ^3He filled proportional chamber. Neutrons convert in the gas in the absorption region. The resulting primary ionization then drifts to the anode plane to undergo multiplication. Position information in X and Y coordinates can be found from the cross-wire cathodes by resistive charge division. Refinement of charge division schemes has led to very large signal to noise ratios (Radeka, 1980), such that the limit to position resolution is solely due to the range of the reaction products shown in figure 3.

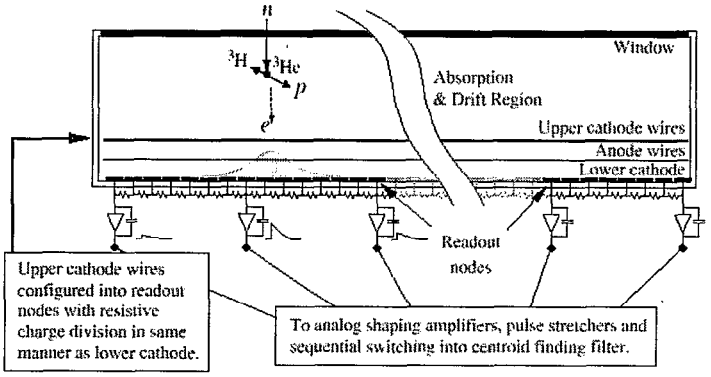

Figure 5. Side-view of proportional chamber with position-readout by resistive charge division.

Gas proportional chambers can be fabricated in a wide range of sizes and configurations, a feature that has made them particularly popular in imaging experiments at the world's reactor and spallation sources. A report by McElhaney (1990) detailing

detectors at these installations indicated nearly all were some form of gas detector. Figure 6 and figure 7 show two detectors from Brookhaven National Laboratory at opposite extremes of the size scale. The first is a planar detector with a sensitive area of 5 cm × 5 cm and the second is a curved detector with a sensitive area of 1.5 m × 20 cm.

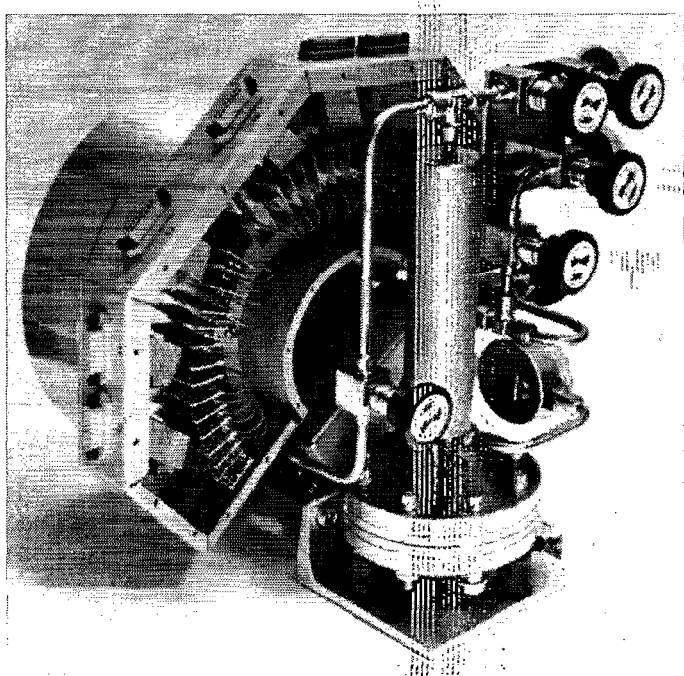

Figure 6. This 5 cm × 5 cm detector has the world's highest neutron resolution in gas, <400 μm FWHM.

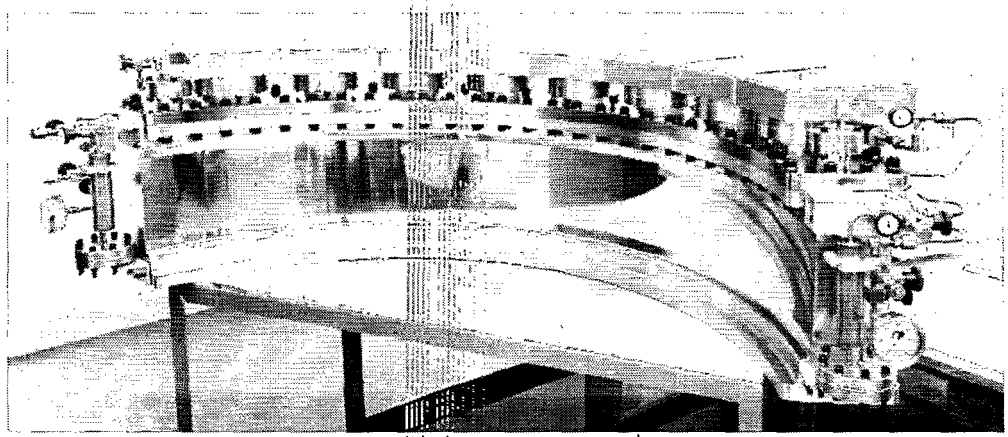

Figure 7. Curved 120° detector for protein crystallography, with sensitive area 1.5 m × 20 cm

Gas-filled detectors are extraordinarily stable over long periods of time when fabricated correctly, and possess very good absolute count rate repeatability. These features permit experiments that would otherwise be almost impossible to carry out. In a study of crystalline domains (Imai, 1997), a non-ionic detergent-water mixture was investigated at constant temperature by time-resolved neutron scattering. Structural oscillations were observed at 5 min intervals by recording the Bragg peaks that speckle the Debye Scherrer ring. One of the many time frames recorded over several days is shown in Figure 9. It is the gas detector's ability to record the time dependence of the

intensity and position that makes a study of this nature unique. Recent examples of gas detector results in structural biology are reported in Schoenborn, 1996.

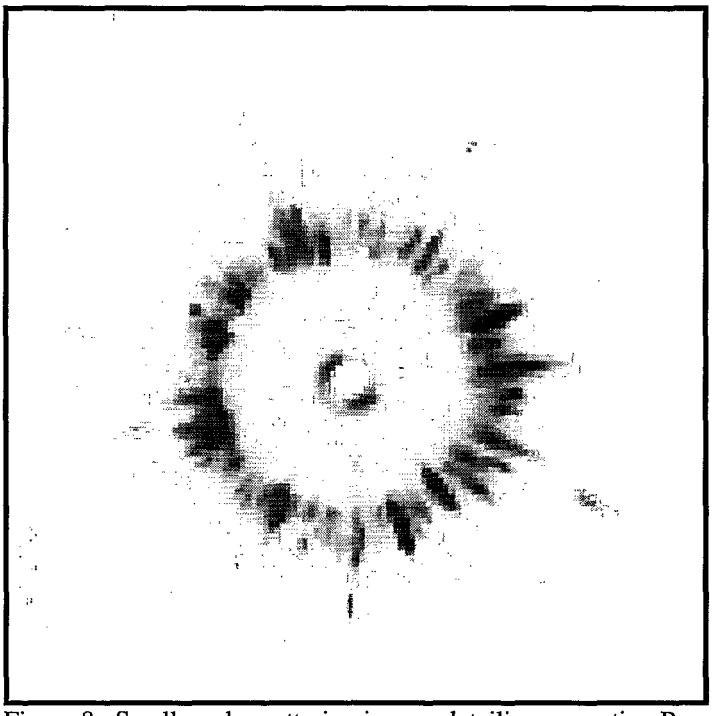

Figure 8. Small-angle scattering image, detailing many tiny Bragg peaks in a Debye Scherrer ring.

ii) Discrete Element Counters

Single wire proportional counters (from which the MWPC, above, ultimately was derived) constitute one of the most basic types of neutron detector. They comprise a cylindrical tube (of order cm diameter) with a central anode (which can be 1m or longer), filled with the same gas mixture as the MWPC. An event's position is determined from resistive charge division along the complete length of the anode, using charge amplifiers at each end to measure signal level, Radeka (1974). Although the readout is relatively simple, good position resolution cannot be obtained from long counters (in contrast to the subdivided readout described for MWPCs), the counters have variable efficiency due to their circular cross-section, and generally they have a modest counting rate capability. In arrays, they can be used to cover large areas, but generally are less superior to a MWPC with a uniform thickness gas volume.

iii) Micro-Strip Gas Chambers (MSGCs).

These were developed originally at the Institute Laue Langevin (ILL), Grenoble (Oed, 1988). In the MSGC the anode and cathode wires of a MWPC are replaced by metallic strips on a glass or plastic substrate. These electrodes can be registered with high precision by photolithography, potentially leading to more automated fabrication processes, better position resolution across the anodes and higher count rates.

A section of an anode bounded on each side by a cathode is shown in figure 10. The anode, typically about 10 μm wide, has a field in excess of 3×10^5 V/cm at its surface.

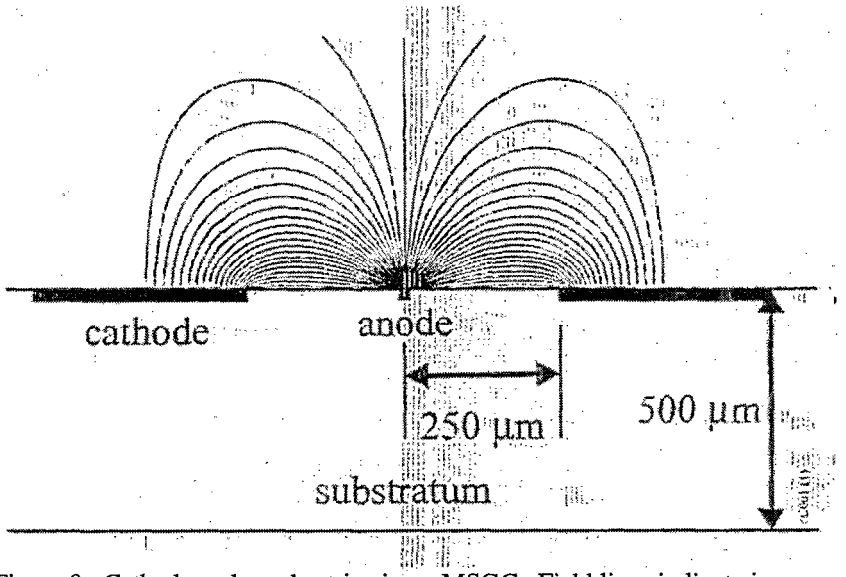

Figure 9. Cathode and anode strips in an MSGC. Field lines indicate increased electric field at anode surface.

Detectors based on the MSGC technology have been developed extensively for neutron detection at ILL. Figure 10 shows one such arrangement of detector. The Micro-Strip (MS) plate is made from Schott S8900 glass, a material that appears to offer long-term resistance to charging problems. The front side, made of a 1500 Å chromium layer, has a pitch of 1mm with anodes of 12 µm and cathodes of 500 µm. Induced signals on these cathodes determine one position coordinate of an event. On the rear side, 86 chromium electrodes, 960 µm wide, are placed perpendicularly to the front structure, for determination of the second position coordinate.

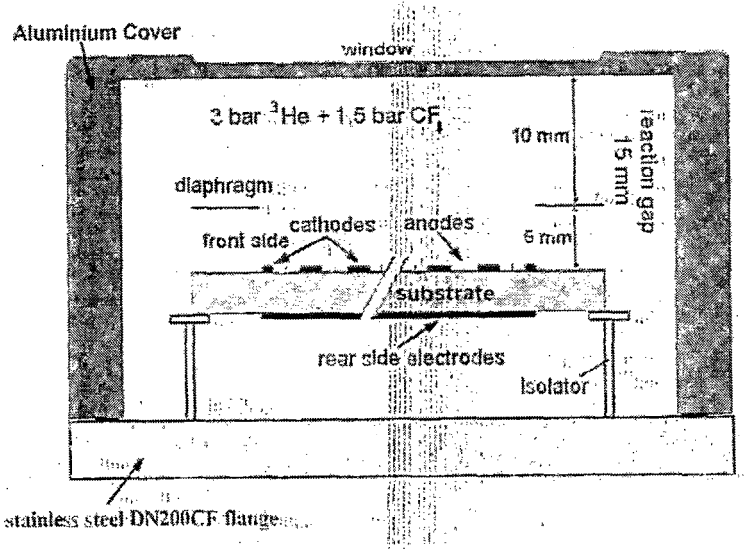

Figure 10. Schematic arrangement of the MSGC detector.

Detectors from ILL have used CF_4 as the stopping gas, and the position resolution achievable is comparable to that with C_3H_8. Figure 11 illustrates the image of a cadmium mask.

The timing resolution of single wire counters, MWPCs and MSGCs is typically of order 1μs. This is primarily due to the uncertainty in the neutron conversion point in several mm of gas, conbined with the slow neutron velocity.

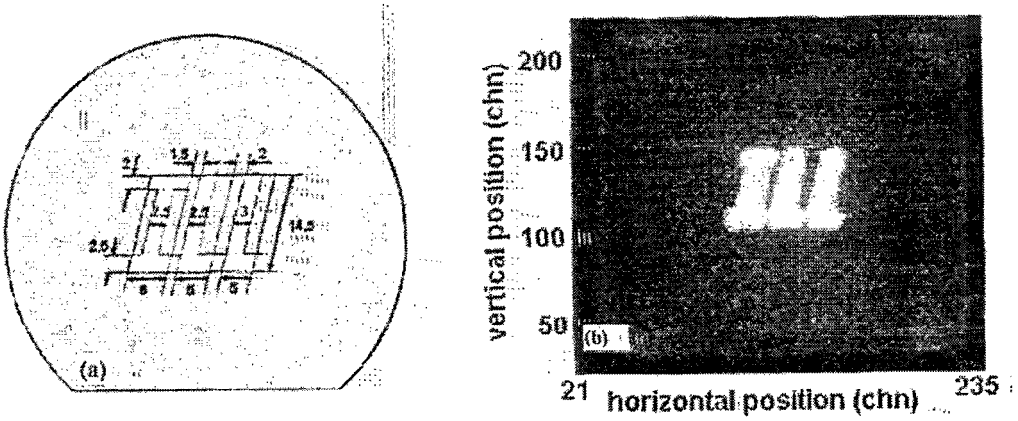

Figure 11. (a) Cadmium mask, with dimensions in mm, (b) Detector image with thermal neutrons.

iv) MSGCs with Gd/CsI converters.

This principle is based on the original work of Dangendorf et al (1994). The technique is being applied in a device which has a Gd foil in the center, a layer of CsI on each side of the foil, and a low-pressure MSGC on both sides to detect the secondary electrons emitted from the CsI (Gebauer, 1997, Gebauer, 1998). The main features of the device, illustrated in figure 12, are as follows. Neutrons convert in a thin Gd foil in the center of the device. Conversion electrons escape into a layer of CsI, on both sides of the foil, and further secondary electrons are emitted from this because a high electric field is present. These electrons drift across a low-pressure gas region to two-dimensional MSGCs on each side. This device has inherent resolution of less than 100 μm, high count rate capability and excellent timing. No working devices have yet been reported. The timing resolution of this device is expected to be at least an order of magnitude smaller than the conventional gas detector because the neutron conversion takes place in a very thin foil.

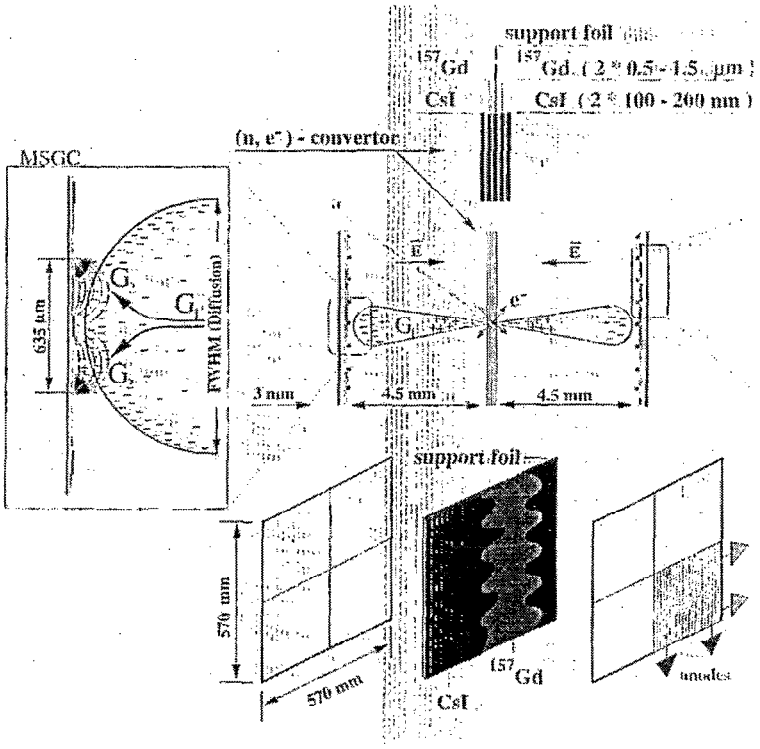

Figure 12. Principle of proposal for neutron imaging with Gd/CsI and low pressure operation of MSGCs.

4. Scintillator Detectors.

Solid state scintillators are about three orders of magnitude higher in density than gases at atmospheric pressure, and in general have much greater stopping power per unit volume. ^{6}Li based materials are by far the most common. Table 2 gives the characteristics of the main solid state scintillators (Knitel, 1998).

Table 2
Characteristics of Solid State Scintillators

Material	Li concentration (cm^{-3})	Photons / absorbed neutron	Decay time (ns)	λ (nm)
^{6}Li-glass:Ce^{3+}	2×10^{22}	6,000-7,000	75	395
^{6}LiI:Eu^{2+}	1.8×10^{23}	51,000	1.4×10^3	470
^{6}LiF/ZnS:Ag^+	1.2×10^{22}	160,000	10^3	450
^{6}Li glass:Tb^{3+}	3×10^{22}	45,000	3×10^6	550
Gd_2SiO_5:Ce^{3+}	-	800	56/600	430

i) Anger Cameras.

Originally conceived for X-rays, the Anger camera (Anger, 1958) became an attractive option for neutrons through developments at Argonne National Laboratory (Strauss, 1981). It consists of a single sheet of scintillator material, an intermediate layer to disperse the light, and an array of photomultiplier (PM) tubes, see figure 13. A

neutron conversion in the scintillator creates light that is seen by a group of neighboring PM tubes, and a center of gravity calculation is performed from the amplitude information from the respective tubes. Most commonly used scintillators are those based on ^{6}Li-glass:Ce^{3+}, available from vendors such as Bicron.

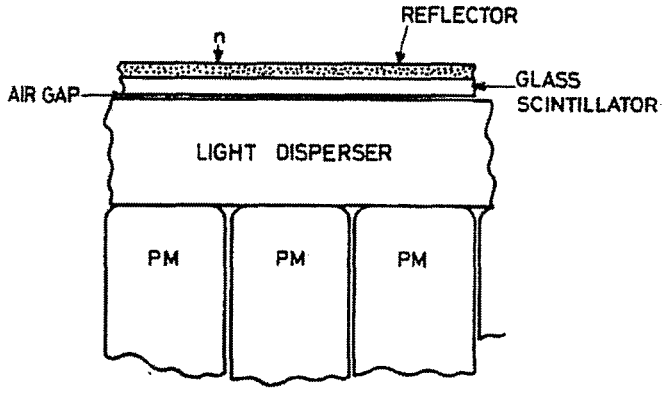

Figure 13. Schematic of the Anger Camera

Kurz (1988) describes further work on Anger cameras, and Schafer (1995) describes linear and area detectors readout both as Anger cameras and with position-sensitive photmultipliers. These devices achieve relatively high counting rates and have good timing because of the thin layers. A major disadvantage is a relatively high gamma sensitivity.

A device with ^{6}Li glass and microchannel plate will be described in section 7.

ii) Scintillators with fiber optic coding.

This technique was first demonstrated about 20 years ago (Davidson, 1983). The principle is shown in figure 14. The light produced by neutron capture in the scintillator

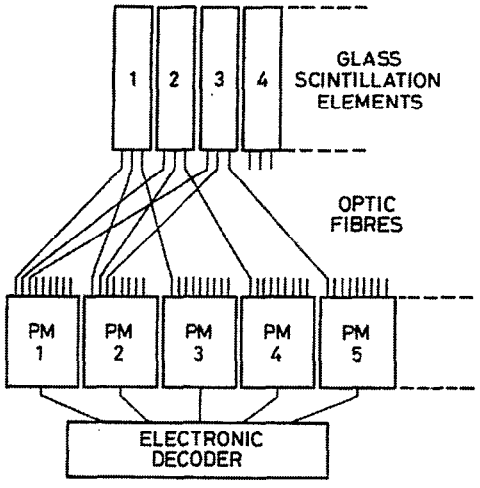

Figure 14. Fiber-optic coding of a discrete element scintillator detector.

is divided between three fiber optic channels, and coupled uniquely to a combination of three PM tubes. The major advantage is a reduction in the number of PM tubes required compared with the number of resolution elements. This technique has been further developed at the spallation facility ISIS, located at the Rutherford Appleton Laboratory. Initially used with linear detector arrays using $^{2}C_{n}$ coding, devices have now been developed using $^{4}C_{n}$ coding that yield two-dimensional information.

A recent example at ISIS of a two-dimensional device based on this coding principle (Rhodes, 1997) is a detector designed for a new diffractometer, where the requirement was for a square detector of dimensions 500 mm × 500 mm with a pixel size of order 10 mm × 10 mm. This detector was designed as four modules, with each module having an active surface area of 348 mm × 144 mm.

A single module consists of a scintillator of ZnS/ ^{6}Li coupled by fiber optics to an array of photomultiplier tubes. The scintillator is located in front of an aluminized mylar, light guide grid that divides the module into 348 pixels, arranged on a 29 × 12 array, with pixel size 12 mm × 12 mm. Figure 15 shows a single module from which the light tight cover has been removed, and in which the scintillator has been removed (it is lying on the

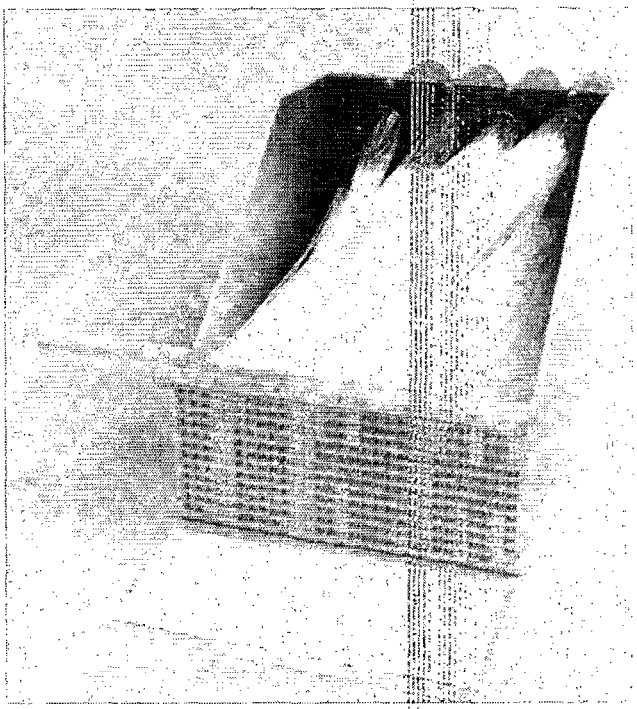

Figure 15. One module of the coded scintillator/fiber optic device. Pixel array is 29 × 12. One PM has been removed and its fibers illuminated (from rear). Beginning at bottom of right hand column, first pixel (lit) contains fibers from PMs 1, 2, 3 and 4, the next one up (dark) from PMs 1, 2, 3 and 5, all the way (all dark) to the ninth pixel up, PMs 1, 2, 3 and 12. The tenth pixel up (lit) contains fibers from PMs 1, 2, 4 and 5, the eleventh (lit) PMs 1, 2, 4 and 6 and so on. Thus, it is PM 4 that is illuminated.

floor) to reveal the pixel array. Each pixel is viewed by sixteen 1.5 mm diameter, fiber optic light guides. These fibers are optically bonded to PM tubes at the rear of the module, using a $^{4}C_{n}$ code. (Every pixel is actually a 2×2 array of square cells, each 6×6 mm^{2}. Centered on each cell are four fibers, and corresponding fibers from each cell join at the appropriate PM tube). For example, the first pixel is coupled to PMs 1, 2, 3 and 4,

the second pixel is coupled to PMs 1, 2, 3 and 5 and so on. In this way, all 348 pixels of a module are coded by just 12 PMs. In figure 15, one photomultiplier tube has been removed and its fiber optic bundle illuminated, thereby highlighting those fibers that feed that particular PM.

Outputs from the photomultiplier tubes are amplified and registered by discriminators, whose outputs are fed to a decoder. This EPROM generates the appropriate binary address for each unique set of four coincident inputs. After time stamping, a histogramming memory is updated. Table 3 shows the major characteristics of this device.

Table 3
Detector Characteristics of Two-dimensional Fiber Coded Scintillator Detector

Active Surface	348×144 mm^2	# of Photomultipliers	12
# of Pixels	348	Diameter	51 mm
Pixel Dimension	12×12 mm^2	Neutron Efficiency @ 1 Å	20%
# of fibers/module	5568	Gamma Sensitivity/^{60}Co	$<10^{-8}$
Fiber diameter	1.5 mm	Background cts (cm^{-2} h^{-1})	0.7
Fiber code	^4C_n	Pulse Pair Resolution	2.5 μs

There is an interesting development with a new material based on Li/Gd borate (Czirr, 2001). Initial measurements with small samples indicate a pulse height distribution for neutrons that is much more spectroscopic than existing scintillators, and offering better n,γ discrimination. No imaging developments have yet been reported.

5. Semiconductor Detectors.

The use of semiconductors in neutron detection generally requires conversion of the neutron in a foil. The charged particle that may escape from the foil is sensed by the semiconductor. Foils can be used in transmission, as illustrated in figure 16, in backscatter mode, or both. However, this technique is a delicate and somewhat nature-dependent compromise: the foil should be sufficiently thick for high conversion efficiency, yet thin enough to allow secondary particles to escape.

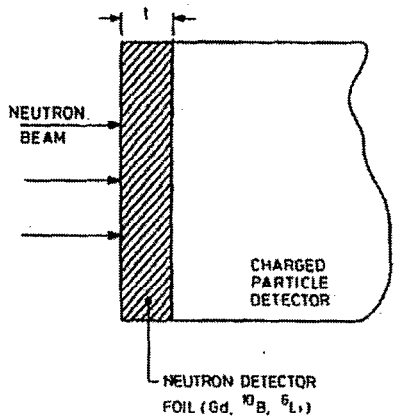

Figure 16. Principle of foil converters in transmission mode.

Figure 17 illustrates the efficiencies of ^{157}Gd and ^{nat}Gd for 1Å neutrons, as a function of foil thickness. Efficiency in this instance means that the probability of an escaping electron is unity. It should be noted that the foil thicknesses are very small, and the efficiencies are not very high. (It is clear from this diagram why the Gd foil in the case of the MSGC/Gd detector described in section 3(ii) is so thin.). These detectors have generally very good timing resolution because the secondary emission and its solid state detection is extremely prompt.

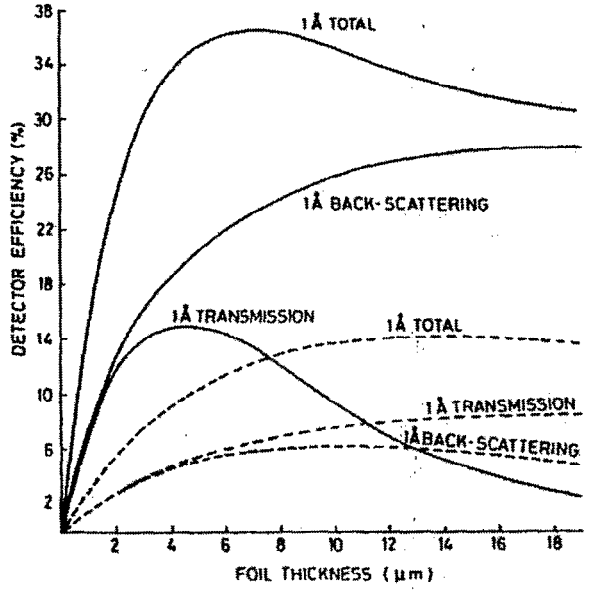

Figure 17. Detection efficiency as a function of foil thickness (solid line: ^{157}Gd; dashed line: ^{nat}Gd).

i) Silicon Semiconductor with ^{6}LiF converter

In this approach (Schelten, 1997) a layer of LiF is attached to a reverse-biased Si diode. The reaction products are an alpha, which has a range of only a few μm, and a triton, which has several times the alpha range. Even if only half of its 2.7 MeV is dissipated in the silicon, 3.8×10^5 electron/hole pairs are created, a sizeable signal. Such a LiF/Si device was made into a linear position-sensitive detector by fabricating one of the two main electrodes as 24 strips of 1.25 mm spacing, and connecting them to an RC line. This application of charge division permits position determination, and a measured spatial resolution of 1.25 mm has been obtained (Schelten, 1997). The relatively thin converter layers (16μm) yield less than 10% neutron absorption probability, and further work is necessary to render this technique more practical.

ii) Silicon/Gd Microstrip.

A Si microstrip detector, a thin wafer of fully depleted silicon with readout strips on one face that permits position determination, has been coupled to a Gd converter (Petrillo, 1999), as shown in figure 18.

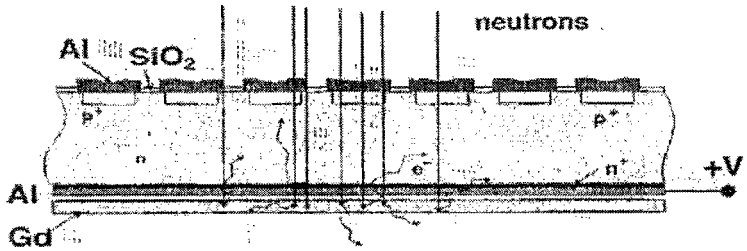

Figure 18 Principle of the Gd converter and silicon strip detector

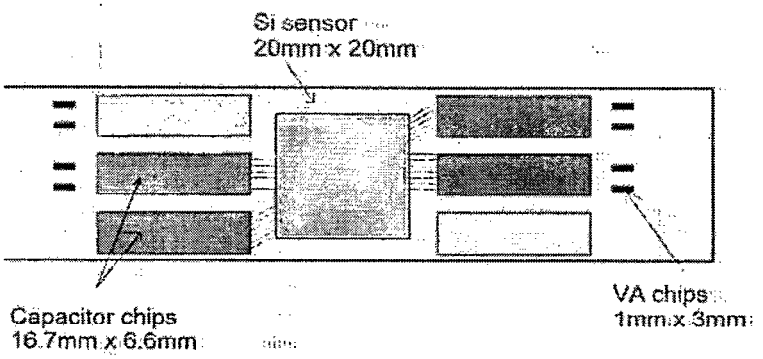

Figure 19. Silicon microstrip detector readout set-up

In recent work on this type of instrument, a double-sided microstrip silicon sensor with area 20×20 mm^2 size was used. This is shown in figure 19. Signals from the 400 μm pitch strips are fed to low noise charge-sensitive preamplifier/shaping amplifier (VA) chips, the channel with the largest signal being representative of the position of a specific event. The neutron converter was a 250 μm thick natural Gd foil mounted in contact with the back-plane of the sensor. The less energetic line of the conversion electron spectra following neutron capture in Gd is observed at about 70 keV, creating about 2×10^4 electrons in the silicon. This is relatively easily detectable by the electronics.

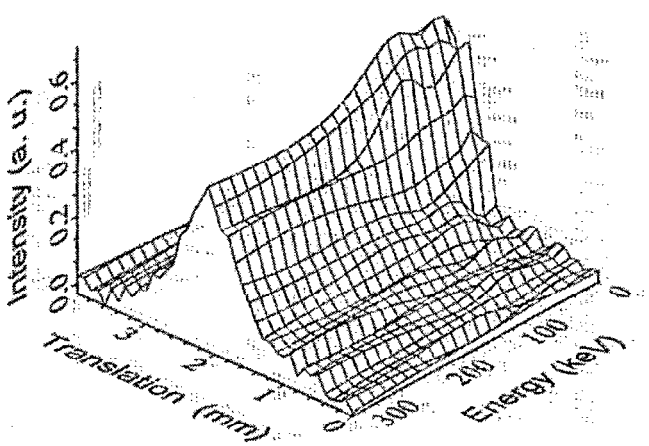

Figure 20. Position response as a function of neutron energy.

Figure 20 shows the position response, which was measured by scanning a beam of neutrons from the TRIGA reactor, Italy, across the detector. By selecting monochromatic neutrons, position response as a function of energy was also determined, and a small dependence upon neutron energy is observed. It is likely that γ-ray background plays a limiting role in these measurements.

Timing resolution of semiconductor-based detectors should be of order a few ns.

6. Film and Image Plates

i) Film.

Thermal neutrons can be imaged with high resolution by photographic film. Diffraction experiments with film were carried out many years ago (Wollan, 1948), using indium as the neutron absorbing medium. Now, the secondary foil is usually Gd. An alternative approach is to use a scintillator, such as ^{6}LiF/ZnS. A system has been described (Hohlwein, 1983) in which film is sandwiched between two such screens, and a resolution of 100μm was obtained. Although film consists of silver halide grains of order 5 μm in size, this intrinsic resolution is rarely achieved because the range of the electron from the foil is typically much longer. Film, like the Image Plate (next section), has the advantage of low cost, ability to cover large areas, flexibility, and good resolution. The disadvantages are no timing information, no sensitivity to single neutrons and the inconvenience of a two-step readout process. Photographic film has a much smaller dynamic range, about 100:1, compared to Image Plates.

ii) Image Plates.

Image Plates (IPs) were developed for diagnostic radiology during the early 1980s (Sonoda, 1983). They were soon used widely in X-ray protein crystallography (Amemiya, 1988). An IP is about 0.5 mm thick and is composed of a flexible plastic backing coated with fine storage phosphor crystals ($BaFBr:Eu^{2+}$) combined with an organic binder. The phosphor is capable of storing part of the energy released when ionizing radiation converts in the plate. When the plate is later stimulated by visible light, photostimulated luminescence (PSL) is emitted, whose intensity is proportional to the neutron dose. Essentially the IP is a form of electronic film, in which incoming radiation creates an integrated latent image that is subsequently read out. The image is retrieved by illuminating the plate with laser light (HeNe); this produces PSL, or characteristic fluorescence radiation, from Eu^{2+}. The number of photons emitted is proportional to the converted incident radiation. A convenient method to perform the readout is a raster scan with a laser beam, simultaneously feeding the fluorescence radiation through a fiber-optic cable to a photomultiplier. IPs have a resolution less than 100 μm, and a dynamic range much greater than that of film, typically 10^5 : 1. These are impressive characteristics. Figure 21 illustrates the readout process for an IP.

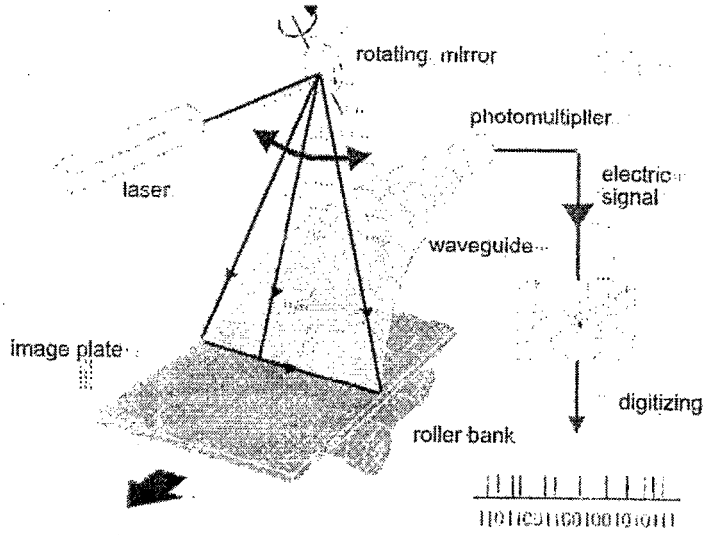

Figure 21. Signal Readout for Image Plate

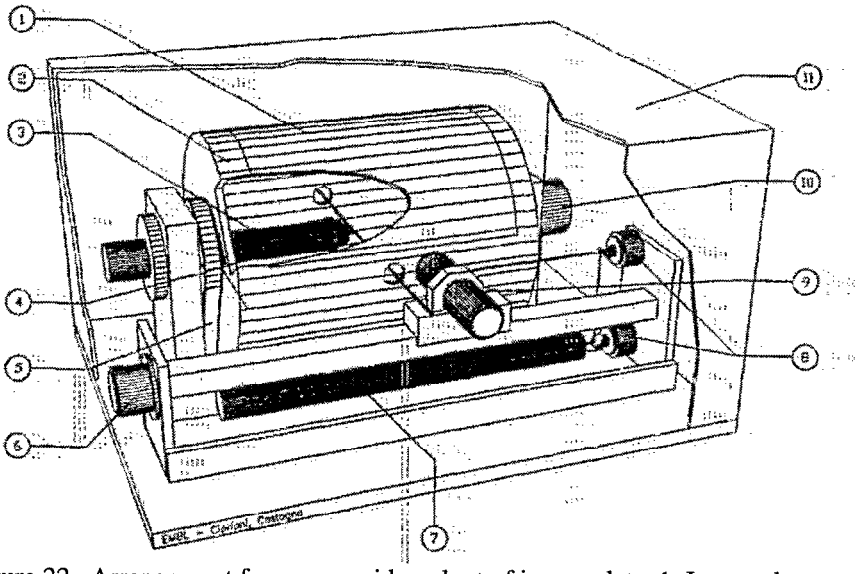
Figure 22. Arrangement for more rapid readout of image plate. 1: Image plate mounted on drum. 2: Drum. 3: Sample holder. 4: Crystal. 5: Belt to drive drum. 6: Carrier for read head with photomultiplier. 7: Laser. 8: Mirror to bring laser light to read head. 9: Read head with photomultiplier. 10: Encoder. 11: Cover.

Gadolinium is a good candidate to make an IP sensitive to neutrons. The strong (n,γ) resonance produces a wide range of keV γ-rays, and a cascade of conversion electrons. Both can stimulate the phosphor. The conversion process can be done either by placing a thin plate containing gadolinium in front of the IP or by having the gadolinium compound inside the phosphor. It has been found that the second approach is better both from a resolution and signal to noise viewpoint. (Cipriani, 1995; Knitel, 2000). A key advantage of image plates is their mechanical flexibility. For example, they can be used to surround objects cylindrically as shown in figure 22. In this example, the image plate is mounted on a 30cm drum with the sample inside, on axis. With a pixel size 0.25×0.25 mm^2, about 6 Mpixels were readout in 5 min. A diffraction pattern from

partially deuterated tetragonal lysosyme crystal taken with this instrument is shown in figure 23 (Cipriani, 1997). Recently, it has been shown (Thoms, 1999) that mixing ^{6}LiF into the image plate phosphor may significantly improve the neutron to γ sensitivity by an order of magnitude.

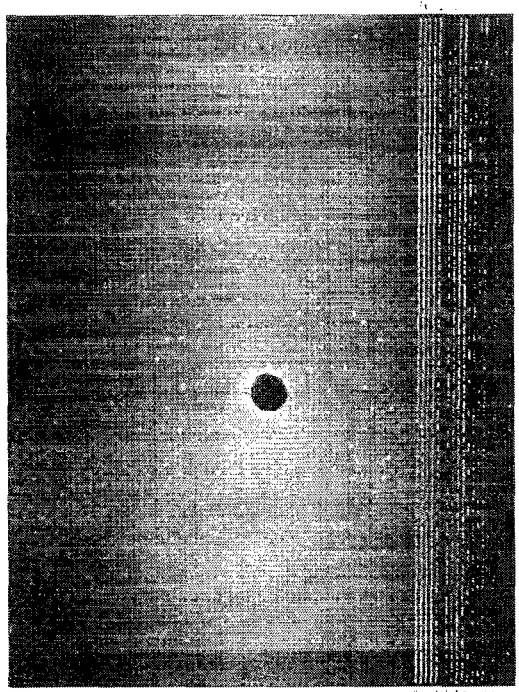

Figure 23. A diffraction pattern from partially deuterated tetragonal lysosyme crystal

7. Microchannel Plates.

Microchannel plates (MCPs) are vacuum imaging devices for UV/X-ray photons and charged particles (Wiza, 1979). A limited amount of work has been carried out to determine their viability as direct detectors of neutrons. A first approach involved measurements with MCPs made from lead-oxide glass containing lithium (Fraser, 1990), where ionization from the emitted α particle is detected. Only a tiny efficiency for neutron detection was measured and, furthermore, it was realized that incorporation of large mole fractions of lithium oxide into MCP lead glass was a severe challenge. A more practical approach is to consider incorporating boron oxide into the MCP glass (Fraser, 1995), but no results have so far been published. A recent development of the microchannel plate, called the microsphere detector, is described (Tremsin, 1996). The outer geometry and appearance of the two devices are essentially identical, but the newer device comprises irregularly packed, sintered glass beads in which an electron avalanche propagates in the gaps between the spheres. So far, however, there appear to be no development of this plate specifically for neutrons.

A combination of scintillator, ^{6}Li-glass:Ce^{3+}, and MCP has been examined as a position-sensitive detector (Schrack, 1984), where the readout was by a two-dimensional resistive sheet. Figure 24 illustrates the principle. In a further development of this

approach, a position resolution of 40 μm has been reported (Rausch, 1996) on a small device.

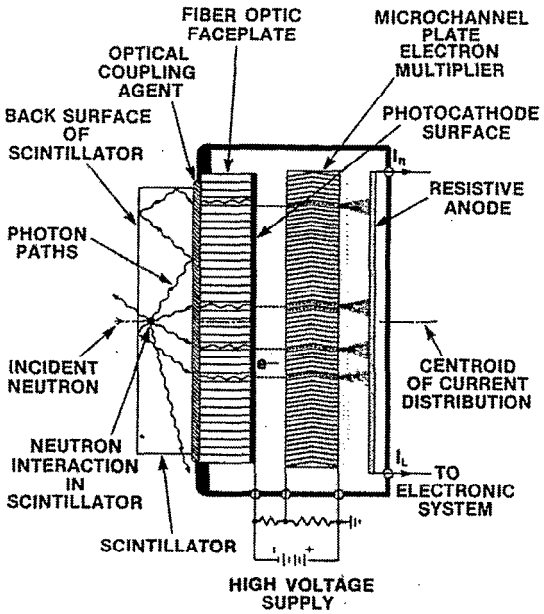

Figure 24. Combination of ^{6}Li glass with a microchannel plate and resistive sheet readout.

8. Radiography and Tomography.

Neutrons have unique scattering and absorption properties for the study of structures and flaws in non-destructive testing of materials. X-rays have a cross-section for absorption that increases approximately as Z^4, and hence they are strongly absorbed by heavy elements and little absorbed by light elements. Low energy neutrons, on the other hand, can interact strongly with light elements and minimally with heavy elements, and can have interaction properties that are several orders of magnitude different between nuclei with close atomic numbers. An excellent selection of papers relating to radiography and tomography with neutrons can be found in Fischer (1996) and (Lehmann, 1999).

Planar neutron radiography was developed to take advantage of these unique neutron properties. It is ideally suited to studies of thin layers. In aluminum, for example, early corrosive changes that are rich in hydrogen-containing compounds can be detected because of the large interaction cross-section with hydrogen nuclei. Neutron radiography, even though it is expensive in comparison with other non-destructive testing methods, is an indispensable part of inspection and examination in fields such as nuclear engineering, aerospace industry, pyrotechnics, oil industry and archeology. Specific examples are:

- welding seams,
- cooling channels in turbine blades,
- gluing of sandwich structures used in aviation,
- homogeneity of new materials or enclosures inside them,
- detection of hydrocarbonates inside metal or ceramic housings.

It has also been used in life science application such as root activity in growing plants (Furukawa, 1999), insect research (Allee, 1996) and the study of microorganisms (Wacha, 2000).

However, the image in radiography is produced from the integrated interaction cross-section over the entire path of radiation through the object. Local density or material changes can be hidden because of this essential averaging. Image reconstruction from a multitude of projections permits tomography to generate three-dimensional detail of the object's internal structure. Some early advantageous features of tomography were realized in test measurements on nuclear fuel (Barton, 1977), but its full potential has been thwarted by lack of efficient, high resolution (fraction of a mm) detectors.

Detectors for radiography have been largely based around image plates, e.g. Stade 1996, Tazaki, 1999, Bayon, 1999, Fujine, 1999). However, image plates (and film) are not practical for tomography because a large number of projections need to be taken in a reasonable time, and need to be available in digital form for further processing. Most tomography work has been based on neutron scintillators coupled to CCDs, eg, McFarland, 1991, Schillinger 1996, Gibbons, 1999, Schillinger 1999, and two are described below.

a) McFarland et al. (McFarland, 1991) at the Massachusetts Institute of Technology pioneered the use of a scintillator screen coupled to a CCD to demonstrate that such a system had the position resolution and efficiency capable of yielding useful tomographs. Figure 25 shows a schematic of the experimental set-up.

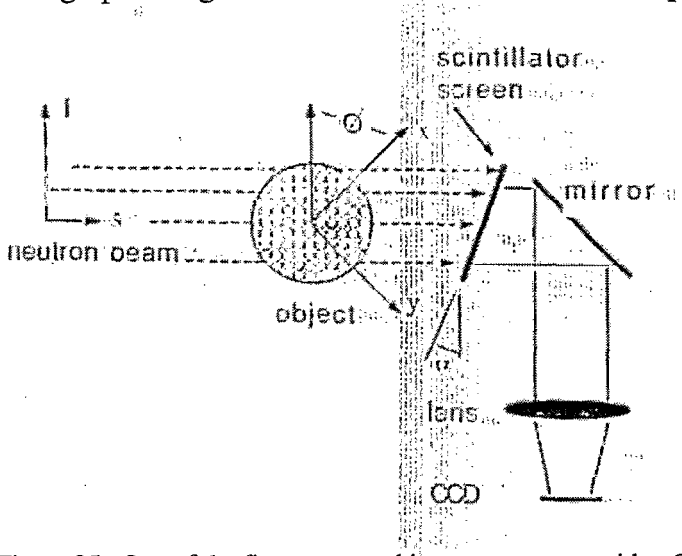

Figure 25. One of the first tomographic measurements with a CCD detector. Neutrons pass through object and are converted in scintillator screen mounted on the inside of a light-tight box. Optical photons reflected from the mirror are focused by the lens onto a CCD.

Neutrons that have passed through the test object convert in the screen, a ^{6}LiF-ZnS scintillator, whose light output is imaged onto a cooled CCD by a front-surfaced mirror and lens. This geometry allows the CCD to be shielded from the incident neutron beam, preventing radiation damage to the CCD and possible neutron activation. Nuclear Enterprises claim an efficiency of 15% for thermal neutrons and a resolution of about 100 μm for the screen, but this specific set-up had significantly lower efficiency because of mismatching of the blue ZnS phosphor and the lens aperture. However, acceptable

images were obtained. Figure 26 shows a neutron tomogram of a small brass control valve (about 3 cm outside dimension) reconstructed from 90 projections at 2° increments. The total imaging time was a little under 5 minutes, with a neutron fluence of 7×10^8 n/cm^2 per projection. Intrinsic resolution is close to the 100 μm of the scintillator.

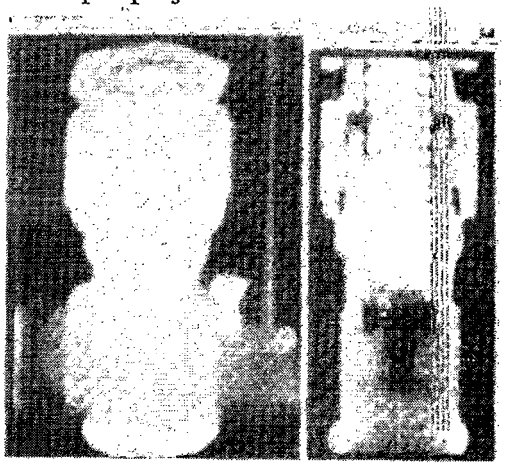

Figure 26. Three-dimensional view of neutron tomographic reconstruction of brass control valve.

b) A group at the Technical University, Munich has developed a high sensitivity CCD camera for detection of the faint light of a neutron scintillator (Schillinger 1996, 1999). A prototype with an active area of up to 28x28 cm^2 has been developed. It is expected that after some further improvements, this detector will be sensitive enough to detect even a few single neutrons on an area as large as 0.5x 0.5 m^2.

As in (a), a commercially available granular scintillator consisting of ZnS(Ag) +^{6}LiF was used. Thermal neutrons are absorbed with an efficiency of about 15 %, and the ionizing reaction products produce approximately 1.8 . 10^5 photons in the ZnS(Ag) crystals with an average wavelength of 470 nm. The product particles, an α and triton, have average ranges of 10 μm and 26 μm respectively within the scintillator. The granular composition of the scintillator limits the resolution to about 50 um.

The efficiency is improved for sub-thermal neutrons as the absorption cross section is inversely proportional to the neutron velocity. The scintillator material itself is somewhat opaque to its own radiation, so the scintillator layer must not be thicker than 0.5 mm for optimum light output, though a thicker layer would be required for optimum neutron absorption. Light output for gamma rays is 450 to 4500 times smaller than for one detected neutron.

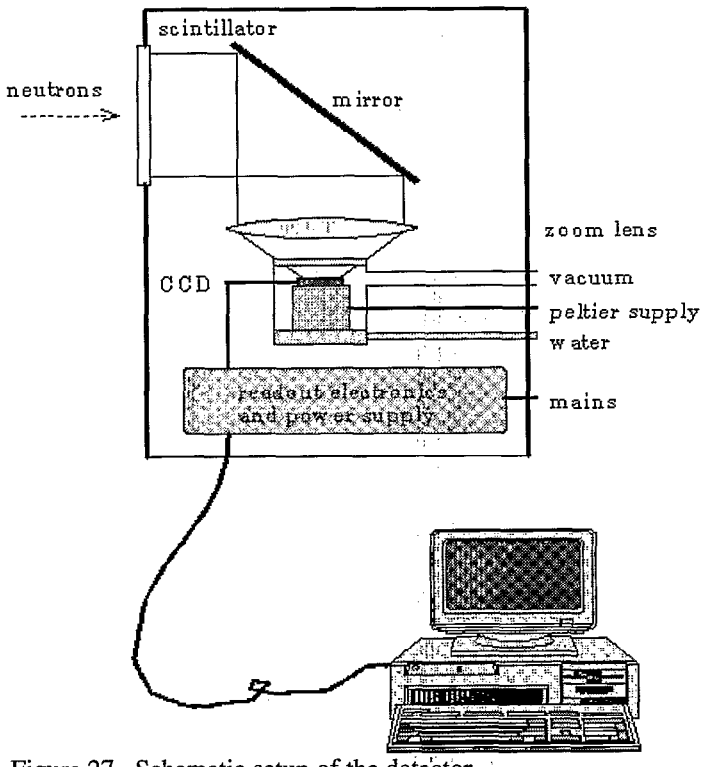

Figure 27. Schematic setup of the detector

Figure 27 shows the set-up of the Munich instrument. The detector consists of a 28×28 cm^2 scintillator screen, an aluminum coated surface mirror and a Peltier cooled CCD camera system with a 512×512 pixel Thomson CCD (TH7895 with 19×19 μm^2 pixel size). The driving electronics are very flexible and compact due to use of highly integrated chips. Control of exposure, read-out and data transfer is performed by a standard PC. As in (a), the scintillator screen is viewed via the mirror by the CCD chip to prevent radiation damage to the latter. The mirror and the backside of the detector housing are transparent for neutrons, so that the non-absorbed part of the beam leaves the detector. A zoom lens with f=1.0 permits coverage of the whole active area of 28×28 cm^2.

Although the CCD is not in the direct line of neutrons, some problems arise from stray gamma rays that are generated by neutron capture in the beam catcher or in the sample. While the light output of the scintillator is negligible for gammas compared to neutrons, the CCD chip itself is highly sensitive to gammas. A gamma event in a CCD generates several thousand photo-electrons and forms a nearly perfect point source. These gamma events appear as isolated bright spots in the picture and can be eliminated by electronic image processing by comparing two identical exposures. In future, the CCD will be shielded with lead glass.

Neutron exposures have been taken at the Garching reactor FRM-I in a flux of order 3.0×10^5 n/s/cm^2, and with an average neutron energy of 6.5 meV. Because the beam was only about 2.5 cm wide and 16 cm high, large-area pictures were obtained by mounting the detector and sample on a translation table, which was scanned across the beam. A compete radiograph was taken in ten minutes, exposing each parts of the sample to the beam for two minutes.

Figure 28 shows a radiograph of a car ignition distributor. On top is the low pressure box for ignition time adjustment, with a steel spring and membrane, and below this is the plastic housing of the capacitor, nearly dark because of its hydrogen content.

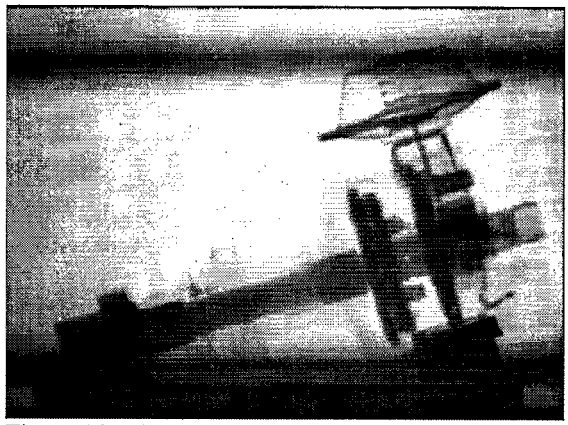

Figure 28 The raw data of a car ignition distributor.

An example of the transformation from projection to tomograph is shown in figure 29. The object is a small electromotor about 20 mm in diameter. The CCD instrument was used to record 200 projections in 0.9° steps with three minutes exposure each time, totaling about 12 hrs including data transfer. One such projection is shown in figure 29(a). From all projections, a three-dimensional reconstruction can be put together from a stack of two-dimensional reconstructions, the latter in turn being obtained from Fourier analysis of the projection raw data (Kak, 1988). The three dimensional reconstruction was put together from 268 separately reconstructed layers of 201 ×201 pixels, forming a data cube of 201 × 201 × 268 pixels, figure 29(b). Each 3D pixel corresponds to a cube of side about 120 μm.

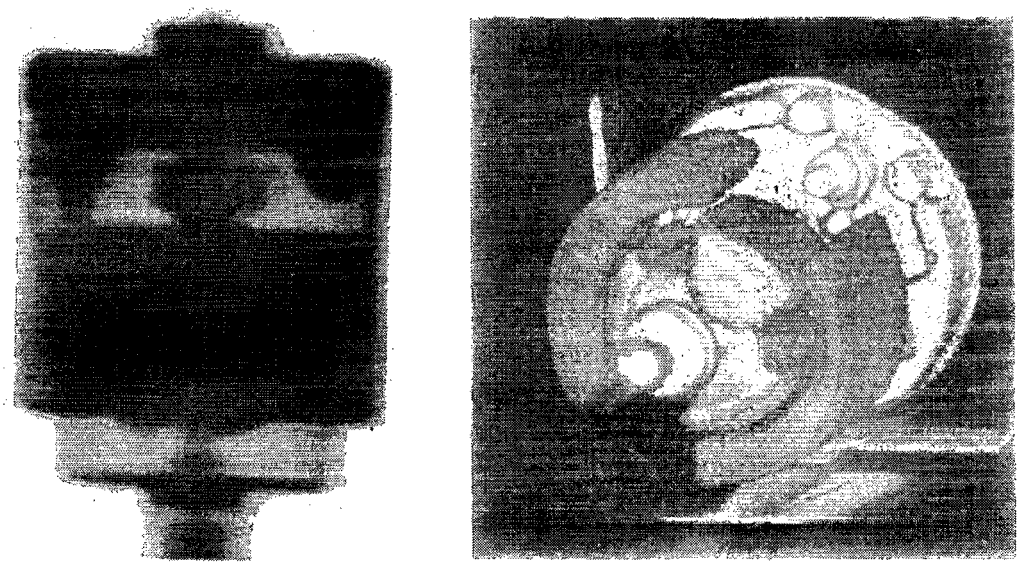

a) b)

Figure 29. Neutron radiography/tomography of small motor.
a) One single projection, b) Front view of motor (268 reconstruction layers).

Some upgrades to the detector system that will improve both throughput and image quality are a reduction of dark current noise by liquid nitrogen cooling, improvement of the sensitivity of the CCD for the 470 nm scintillation light by coating with laser dyes, which act as wavelength shifters, or by usage of backlit CCDs. Better shielding against gamma rays and better light collection with high-aperture lenses (F=0.75) and fiber optic tapers are also being planned.

Fast neutron radiography is an attractive non-destructive inspection technique because of the excellent penetration characteristics of fast neutrons in matter. The difficulty of detecting fast neutrons, however reduces its attractiveness. Some techniques have been developed to help overcome this difficulty. Two image plates and a sheet of polyethylene as a proton emitter was examined (Masahito, 2001), with results that showed the method could be applicable to fast neutron radiography with effective discrimination of γ-rays.

9. Closing Remarks.

In this article, we have described the principle reactions in nature that are useful for detection of neutrons, highlighted the salient features of a range of detector technologies that have been developed for imaging purposes, and outlined an important application, namely radiography and tomography. However, in covering quite a range of disparate technologies, it is not possible to delve too deeply into some fundamental aspects of radiation detection. For example, in describing each imaging technology, little distinction has been made between single neutron counting and integrating mode. In fact, there are only three detector types described in this article that are truly integrating, namely film, the image plate (section 6), and the combination of scintillator and CCD (section 8). These are most useful in very high rate applications where an image can be recorded quickly and where no time resolution is required; hence they are commonly used in radiography and tomography. All other detector types described register neutrons electronically, one event at a time. This offers the possibility of time tagging events and, in experiments at spallation sources, each neutron energy can then be determined. Thermal neutrons, particularly, move very slowly; 1 meV and 100 meV neutrons traverse 10m in 23ms and 2.3ms respectively. Flight paths between source and detector can easily be 10m, and therefore time differences of several milliseconds can occur between the arrival of the least, and most, energetic neutron from one spallation pulse. Timing resolution, non-existent for integrating detectors, has been indicated for counting detectors where appropriate.

Development of improved neutron imaging techniques will continue to be an area of challenging research. Detectors with sub-mm resolution, counting rates of MHz per cm^2, and area coverage of several m^2 are essential if the world community is to make effective use of the newest spallation sources now under construction and consideration throughout the world.

Ackowledgements.

The author would like to acknowledge many informative discussions with his Brookhaven colleagues, particularly Drs. Veljko Radeka and Bo Yu, and many other colleagues at neutron facilities in the US and abroad.

References:

Allee, L.L., Davis, P.M. & Aderhold, H.C., (1996). Proc. 5th World Conf. On Neutron Radiography, Eds: C.O. Fischer, J. Stade and W. Bock, Berlin, 728-733.

Amemiya, Y., Matsushita, T., Nakagawa, A., Satow, Y., Miyahara, J., & Chikawa, J., (1988). Design and Performance of an Imaging Plate System for X-ray diffraction Study. Nucl. Instrum. & Meth. **A266,** 645.

Anger, H.O., (1958). Scintillation Camera. Rev. Sci. Instrum. **29,** 27-33.

Barton, C.F., (1977). Computerized Axial Tomography for Neutron Radiography of Nuclear Fuel. Trans. Am. Nucl. Soc. **28,** 212-213.

Bayon, G., (1999). Present applications of neutron radiography in France. Nucl. Instrum. & Meth. **A424,** 92-97.

Boie, R.A., Fischer, J., Inagaki, Y., Merritt, F.C., Okuno, H., Radeka, V. (1982). Two-dimensional high Precision Thermal Neutron Detectors. Nucl. Instrum. & Meth. **200**, 533-545.

Charpak, G, Bouclier, R, Bressani, T, Favier, J &Zupancic, C., (1968). The Use of Multiwire Proportional Counters to Select and Localize Charged Particles. Nucl. Instrum. & Meth. **62,** 262-268.

Cipriani, F., Castagna, J.-C., Lehmann, M.S., & Wilkinson, C., (1995). A large image-plate detector for neutrons. Physica **B 213 & 214,** 975-977.

Convert, P.B. & Forsyth, J.B., Eds. (1983). Position Sensitive Detection of Thermal Neutrons, Academic Press, London.

Crawford, R.K. (1992). Position-sensitive Detection of Slow Neutrons – Survey of Fundamental Principals. Proc. SPIE **1737** 210-223.

Czirr, B., MacGillivray, G.M., MacGillivray, R.R. & Seddon, P.J. (2001). Performance and characteristics of a new scintillator. Nucl. Instrum. & Meth. **A424** 15-19.

Dangendorf, V., Demian, A., Friedrich, H., Wagner, V., Akkerman, A., Breskin, A., Chechik, R. & Gibrekhterman, A. (1994). Thermal neutron imaging detectors combining novel composite foil converters and gaseous electron multipliers. Nucl. Instrum. & Meth. **A350,** 503-510.

Davidson, P.L. & Wroe, H. (1983). Test Results on a Linear PSD using Fibre Optic Encoded Scintillators. In: Position Sensitive Detection of Thermal Neutrons, Convert, P.B. & Forsyth, J.B., Eds. Academic Press, London, 166-174.

Fischer, C.O., Stade, J., Bock, W., Eds. (1996). Proc. 5th World Conference on Neutron Radiography, Berlin, Pub: DGZfp.

Fraser, G.W., & Pearson, J.F., (1990). The Direct Detection of Thermal Neutrons by Imaging Micro-channel Plate Detectors, Nucl. Instrum. & Meth. **A293,** 569-574.

Fraser, G.W., (1995). Thermal Neutron Imaging, Proc. SPIE **2339** (1995) 287-301. (Proc. 4th International Conference on Neutrons and Their Applications).

Fujine, S., Yoneda, K., Kamata, M. & Etoh, M., (1999). Application of Imaging Plate Neutron Detector to Neutron Radiography. Nucl. Instrum. & Meth. **A424**, 200-208.

Furukawa, J., Nakanishi, T.M. & Matsubayashi, M., (1999). Neutron radiography of a root growing in soil with vanadium. Nucl. Instrum. & Meth. **A424**, 116-121.

Garber, D.I. & Kinsey, R.R., (1976) Neutron cross-sections Volume II, curves. Report No. BNL 325, Brookhaven National Laboratory.

Gebauer, B., Schulz, Ch., & Wilpert, T., (1997) Novel large-area thermal neutron imaging detectors comprising ^{157}Gd/CsI convertors and micro-strip gas detectors with low-pressure, two-stage amplification and delay line readout. Nucl. Instrum. & Meth. **A392**, 68-72.

Gebauer, B., Schulz Ch., Wilpert, T., & Biagi, S.F., (1998). Large-area, low-pressure microstrip gas chambers for thermal neutron imaging. Nucl. Instrum. & Meth. **A409**, 56-62.

Gibbons, M.R., Richards, W.J. & Shields, K., (1999). Optimization of neutron tomography for rapid hydrogen concentration inspection of metal castings. Nucl. Instrum. & Meth. **A424**, 53-57.

Groshev, L.V. et al, (1962). Gamma-rays and Conversion Electrons from the (n,γ) Reaction on Gadolinium Isotopes. Bull. Acad. Sci. USSR Phys. Ser. **26** 1127-1146.

Hastings, J., Smith, G.C. & Yu, B., Eds. (1998). Workshop on Neutron Detectors for Spallation Sources. BNL, http://neutronworkshop.bnl.gov/

Holwein, H. (1983). Photographic Methods in Neutron Scattering – A Review. In: Position Sensitive Detection of Thermal Neutrons, Convert, P.B. & Forsyth, J.B., Eds. Academic Press, London, 379-390.

Imai, M., Kto, T., & Schneider, D. (1997). J. Chem. Phys. **106**, 9362.

Kak, A.C. & Slaney, M. (1988). Principles of computerized tomographic imaging. IEEE Inc., New York.

Knitel, M.J., (1998). New Inorganic Scintillators and Storage Phosphors for Detection of Thermal Neutrons. Ph.D. Thesis, Technical University, Delft.

Knitel, M.J., Bom, V.R., Dorenbos, P., van Eijk, C.W.E., Berezovskaya, I., & Dotsenko, V., (2000). The feasibility of boron containing phosphors in thermal neutron image plates, in particular the systems $M_2B_5O_9X:Eu^{2+}$ (M=Ca, Sr, Ba; X=Cl, Br). Part I: simulation of the energy deposition process. Nucl. Instrum. & Meth. **A449**, 578-594.

Knoll, G.F. (1989). Radiation Detection and Measurement, 2nd Edition, Wiley, New York.

Kurz, R. & Schelten, J. (1988). Two-dimensional neutron detector based on a position-sensitive photmultiplier. Nucl. Instrum. & Meth. **A273**, 273.

Lander, G., Ed. (1996). New tools for Neutron Instrumentation. J. Neutron Res. **4**.

Lehmann, E., Pleinert, H., & Körner, S. (1999). Proc. 3rd Int. Topical Meeting on Neutron Radiography, Lucerne, Switzerland, Nucl. Instrum & Meth. **424,** No.1.

Masahito, M., Hibiki, T., Mishima, K., Yoshii, K. & Okamoto, K. (2001). Preliminary examination of the applicability of imaging plates to fast neutron radiography. Nucl. Instr. & Meth. **A 463,** 324-330.

McElhaney, S.A. & Vandermolen, R.I., (1990). Two-Dimensional Position-Sensitive Detectors for Small-Angle Neutron Scattering. Oak Ridge National Laboratory Report ORNL/TM-11557.

McFarland, E.W., Lanza, R.C.& Poulos, G.W. (1991). Multi-dimensional Neutron-computed tomography Using Cooled Charge-coupled Devices. IEEE Trans. Nucl. Sci. **NS-38**, 612-621.

Oed, A., (1988). Position-sensitive detector with micro-strip anode for electron multiplication with gases. Nucl. Instrum. & Meth. **A263**, 351-359.

Petrillo, C., Sacchetti, F., Maehlum, G., & Mancinelli, M., (1999). Space Resolution of a Si/Gd Microstrip as Linear Position-sensitive Detector for Thermal Neutrons. Nucl. Instrum. & Meth. **A424**, 523-532.

Peurrung, A.J., (2000). Recent Developments in Neutron Detection. Nucl. Instrum. & Meth. **A443**, 400-415.

Radeka, V. (1974). Signal, Noise and Resolution in Position-Sensitive Detectors. IEEE Trans. Nucl. Sci. **NS-21**, 51-64.

Radeka, V., & Boie, R.A. (1980). Centroid finding method for position-sensitive detectors. Nucl. Instrum. & Meth. **178**, 543-554.

Radeka, V., Schaknowski, N.A., Smith, G.C. & Yu, B. (1996). High Precision Thermal Neutron Detectors. In: Neutrons in Biology, Eds Schoenborn and Knott, Plenum Press. 57-67.

Rausch, C.R. (1996). Detektoren für thermische Neutronen mit hoher Ortsauflösung. Thesis, Technical University, Munich.

Rhodes, N.J., Wardle, A.G., Boram, A.J. & Johnson, M.W., (1997). Pixelated neutron scintillation detectors using fibre optic coded arrays. Nucl. Instrum. & Meth. **A392**, 315-318.

Schäfer, W., Jansen, E., Will, G., Szepesvary, A., Reinartz, R. & Müller, K.D. (1995). Update on the Jülich linear and area neutron scintillation detectors. Physica **B213 & 214**, 972-974.

Schelten, J., Balzhauser, M., Hongesberg, F., Engels, R., &. Reinhartz, R., (1997). A New Neutron Detector Development Based on Silicon semiconductor and ^{6}LiF Converter. Physica **B 234-236**, 1084-1086.

Schillinger, B., (1996). 3D Computer Tomography with Thermal Neutrons at FRM Garching. J. Neutron Res. **4**, 57-63.

Schillinger, B., Blümluber, W., Fent, A. & Wegner, M., (1999). 3D neutron tomography: Recent developments and first steps towards reverse engineering. Nucl. Instrum. & Meth. **A424**, 58-65.

Schoenborn, B.P. & Knott, R.B. Eds., 1996. Neutrons in Biology, PlenumPress.

Schrack, R.A. (1984). A microchannel plate neutron detector. Nucl. Instrum. & Meth. **222**, 499-601.

Sonoda, M., Takano, M., Miyahara, J., & Kato, H., (1983). Radiology **148**, 833.

Stade, J., Rant, J.J. & Kaling, M., (1996). Proc. 5th World Conference on Neutron Radiography, Eds: C.O. Fischer, J. Stade and W. Bock, Berlin, Pub: DGZfp, 298-306.

Strauss, M.G., Brenner, R., Lynch, F.J. & Morgan C.B. (1981). 2-D Position-Sensitive Scintillation Detector for Neutrons. IEEE Trans. Nucl. Sci. **NS-28**, 800-806.

Tazaki, S., Neriishi, K., Takahashi, K., Etoh, M., Karasawa, Y., Kumazawa, S. & Niimura, N., (1999). Development of a new type of imaging plate for neutron detection. Nucl. Instrum. & Meth. **A424**, 20-25.

Thoms, M., (1999). Neutron detection with imaging plates part II. Detector characteristics. Nucl. Instrum. & Meth. **A424**, 34-39.

Tremsin, A.S., Pearson, J.F., Lees, J.E., and Fraser, G.W. (1996). The Microsphere Plate: A New Type of Electron Multiplier, Nucl. Instrum. & Meth. **A368**, 719-730.

Vellettaz, N., Assaf, J.E., & Oed, A. (1997). Two-dimensional gaseous microstrip detector for thermal neutrons. Nucl. Instrum. & Meth. **A392**, 73-79.

Wacha, R., Crispim, V.R., Lage, C., & D'Arc R. Lopes, J. (2000), Neutron radiography applied to the micro-organisms detection. Radiation Meas. **32**, 159-162.
Wiza, J.L. (1979). Microchannel Plate Detectors. Nucl. Instrum. & Meth. **162** 587-601.
Wollan, E.O., Shull, C.G. & Marney, M.C. (1948). Laue Photography of Neutron Diffraction. Phys. Rev. **73**, 527-528.